Research on Iron Phosphotungstate Catalyzed Microdroplet Reactions Based on Ambient Mass Spectrometry

Ziming Wang

Received March 04, 2024
Accepted August 31, 2025
Electronic access October 30, 2025

Previous studies have studies the addition reaction of 2,4-dihydroxybenzaldehyde and diisopropyl azodicarboxylate with the joint effort of traditional catalysts like $FeCl_3$ and ultraviolet under traditional monitor equipment like NMR or IR, which have many limitations on real time monitoring. This paper reports a synthesis method for the iron-coordinated phosphotungstate $Fe_3PW_9O_{34}$ and provides a detailed characterization of its structure, composition, and molecular mass using techniques such as Fourier transform infrared spectroscopy (FT-IR), X-ray diffraction (XRD), and electrospray ionization mass spectrometry (ESI-MS). The substance and its synthesis route not only valuable in reaction studied in this paper, but also offers huge potential for future applications on catalytic engineering. Additionally, the reaction mechanism for the $Fe_3PW_9O_{34}$-catalyzed addition reaction of 2,4-dihydroxybenzaldehyde and diisopropyl azodicarboxylate under microdroplets conditions was proposed using Ambient mass spectrometry. This reaction does not require the assistance of external conditions other than the catalyst mentioned, offering a simple method for investigating the activation of C-H bonds and the construction of C-N bonds. By studying this reaction, a convenient method with great potential on real time monitoring is proposed.
Keywords: Ambient Mass Spectrometry, Microdroplets, Polyoxometalates, Addition Reaction

Introduction

Microdroplet Chemistry

Water is the most common yet also one of the most fascinating substances. Even a single “drop” of water, only a trillionth of a liter, can significantly accelerate chemical reactions, exhibiting catalytic effects that have left countless scientists in awe [1]. This is the focus of the cutting-edge field of chemistry in recent yearsmicrodroplet chemistry. This emerging field has garnered significant attention because, within microdroplets, reactions that cannot occur spontaneously can take place, and compared to their bulk-phase counterparts, microdroplets can accelerate reactions by several orders of magnitude [2]. By utilizing water microdroplets, some chemical reactions that traditionally require extreme laboratory conditions, such as high temperature and pressure, can be carried out under ambient temperature and pressure. This not only reduces the energy consumption required for chemical reactions but also enhances the safety of the reactions, making chemical synthesis cleaner, more efficient, and safer.

Reaction Monitoring Based on Ambient Mass Spectrometry

In the study of reaction mechanisms, spectroscopic techniques such as ultraviolet-visible (UV-Vis) spectroscopy, infrared (IR) spectroscopy, and nuclear magnetic resonance (NMR) spectroscopy are commonly used [3]. These techniques detect changes in chromophores or functional groups in the substances being analyzed, reflecting the characteristic changes of intermediates and thus capturing the intermediates generated during the reaction and inferring the reaction mechanism. However, some intermediates are highly reactive and short-lived, posing challenges to traditional methods of reaction mechanism studies. Spectroscopic methods have certain limitations in directly observing instantaneous reaction processes. Therefore, the development of new technologies capable of capturing the transient stages of reactions is urgently needed.

Mass spectrometry (MS) is one of the important techniques for obtaining molecular structure information [4]. It can analyze the structural information of multiple substances in a system in a single detection, making it particularly effective for monitoring chemical reactions, capturing reaction intermediates, and studying reaction kinetics. However, traditional mass spectrometry detection methods may be affected by issues such as signal saturation and mass spectrometry contamination due to high-concentration samples [5]. Consequently, traditional methods typically adopt an ”offline” approach, requiring cumbersome sample pretreatment before testing, which increases the difficulty and complexity of detecting transient intermediates.

In recent years, ambient mass spectrometry (AMS) has developed rapidly. Unlike traditional mass spectrometry [6], which relies on strict vacuum systems and complex sample preparation, AMS enables real-time, rapid, in-situ, and highly sensitive analysis of sample states. It simplifies the operation process by directly sampling from the reaction system and rapidly ioniz-

ing the sample. AMS offers unique advantages in monitoring chemical reactions, providing structural information for various unknown and important reaction intermediates, thus offering strong support for researchers in further exploring chemical reaction mechanisms.

Phosphotungstic Heteropolyacid

Heteropoly acids (HPAs)[7] are a unique class of inorganic compounds consisting of transition metal oxide clusters surrounding one or more central heteroatoms, exhibiting diverse structures and rich chemical properties. Due to their strong acidity, high oxidation capacity, and excellent chemical stability, heteropoly acids have played a significant role in catalysis, particularly in homogeneous and heterogeneous catalytic reactions. In recent years, with the growing emphasis on green chemistry, heteropoly acids have been instrumental in promoting environmentally friendly chemical reactions such as oxidation, condensation, and esterification. Their remarkable catalytic performance makes them ideal alternatives to traditional catalysts, helping to reduce harmful byproducts and enhance reaction selectivity and efficiency[8].

Among the various structural types of heteropoly acids, the Keggin and Dawson structures are the most classic[9]. The Keggin structure is characterized by its regular tetrahedral coordination of the central atom and the octahedral transition metal oxygen clusters surrounding the center. The molecular formula is commonly represented as $Hx[EXM_{12}O_{40}]$, where X represents the central heteroatom (e.g., phosphorus (P) or silicon (Si)), and M represents transition metal elements such as molybdenum (Mo) or tungsten (W), which form the peripheral framework. This structure not only possesses high stability but also allows for precise optimization of its physicochemical properties and catalytic activity by adjusting the types and ratios of heteroatoms and metal elements, demonstrating remarkable tunability. With its unique structural characteristics, adjustable catalytic properties, and broad application prospects in green chemistry and energy/environmental fields, the Keggin-type heteropoly acid has become a hotspot in materials science and catalytic chemistry research[10].

Among the Keggin-type heteropoly acids, the phosphotungstate $PW_{12}O_{40}$ has long been a focal point of research due to its stability and excellent performance. This paper reports the synthesis of a simplified structural variant[11], PW_9O_{34}. Compared to the traditional $PW_{12}O_{40}$, PW_9O_{34} contains fewer metal atoms but exhibits higher surface metal coordination activity. This structural simplification endows it with significant potential as a precursor for functionalized materials, such as composites with specific catalytic activity, and drives its application in energy conversion and storage, as well as environmental pollution control.

Furthermore, although Keggin-type heteropoly acids have been widely used in homogeneous and heterogeneous catalysis, they still face certain limitations in fuel cells and electrocatalysis, particularly in terms of conductivity and redox properties[12]. By introducing transition metal ions such as FE^{3+} , Mn^{2+} or Co^{2+}, their catalytic activity and electron transfer capabilities can be significantly enhanced. Additionally, the coordination modification of metals can improve the material's thermal stability, ensuring that the structure remains intact during high-temperature catalysis. Therefore, this study further enhances the application potential of PW_9O_{34} by coordinating it with iron ions[13].

Activation of C-H Bonds for the Construction of C-X Bonds Reactions

The study of C-H activation reactions for the construction of C-X bonds has gradually become an important direction in organic synthesis. By selectively activating C-H bonds, researchers can construct various types of C-X bonds, such as C-Si, C-F, and C-S bonds. This study focuses on activating C-H bonds and introducing nitrogen sources[14], enabling the synthesis of a wide range of nitrogen-containing compounds, including amines, amides, and heterocyclic compounds. These nitrogen-containing compounds hold significant application value in fields such as drug development, materials science, and agricultural chemistry.

In recent years, the widespread use of transition metal catalysts (e.g., palladium, nickel, and rhodium) in C-H activation has provided new pathways for constructing C-N bonds[15]. These catalysts promote the breaking of C-H bonds and react with nitrogen sources to form new C-N bonds by forming metal-carbon intermediates with the reaction substrates. This process not only enhances the selectivity and conversion rate of the reaction but also reduces the need for multiple steps and protection-deprotection procedures commonly required in traditional synthesis methods, significantly improving synthetic efficiency[2]. Additionally, in-depth studies of the reaction mechanism continue to drive the development of this field. Researchers, through computational chemistry and experimental methods, have uncovered the formation mechanisms of metal-nitrogen intermediates and their impact on reaction selectivity. This deeper understanding allows researchers to more effectively control reaction conditions such as temperature, solvents, and atmospheric composition, optimizing the reaction outcomes.

In terms of practical applications, C-H activation for the construction of C-N bonds has shown immense potential in drug synthesis[16]. Many bioactive molecules and drugs contain C-N bonds in their structure, and traditional synthesis methods often require multiple steps and complex operations. By utilizing C-H activation technology, researchers can synthesize these complex molecules in a single-step reaction, significantly increasing synthetic efficiency. The progress in C-H activation reactions for constructing C-N and C-X bonds not only enriches the methods available in organic synthesis but also provides new strategies

for innovation and development in related fields. As catalyst design, reaction mechanism studies, and application examples continue to evolve, we believe that C-H activation reactions will play an increasingly important role in future chemical synthesis, advancing both scientific research and industrial applications[17].

Contribution

The C-N bond is one of the fundamental chemical bonds in living organisms, playing a crucial role in the construction of biomolecules such as amino acids, nucleotides, peptides, and proteins. Organic compounds containing C-N bonds are widely found in nature and have significant applications in materials chemistry, life sciences, and medicine. Benzylamine, as an important nitrogen-containing compound, is commonly found in bioactive natural products and pharmaceutical molecules, and is also a key raw material for many chemical products, deeply impacting daily life. Therefore, the efficient, economical, and environmentally friendly activation of C-H bonds to construct aryl C-N bonds via photocatalysis is of great theoretical significance and has vast practical potential.

In this study, $Fe_3PW_9O_{34}$ was selected as the catalyst, successfully performing an addition reaction between 2,4-dihydroxybenzaldehyde and diisopropyl azo-2,3-dicarboxylate in a microdroplet under ambient pressure without the need for additional catalytic assistance. This process activates C-H bonds and constructs C-N bonds, providing a new approach for the study of C-H activation to construct C-N bonds without relying on external conditions other than catalyst. Schematic diagram of the addition reaction between 2,4-dihydroxybenzaldehyde and azodimethyl acid diisopropyl ester is shown in Fig. 1.

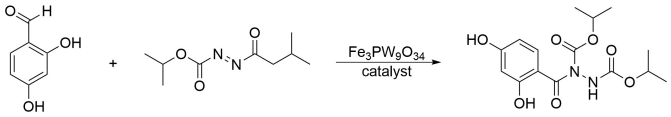

Fig. 1 Schematic diagram of the addition reaction between 2,4-dihydroxybenzaldehyde and azodimethyl acid diisopropyl ester.

Research Methods

Experimental Methods

Synthesis of Basic Iron Acetate

Dissolve $FeCl_3 \cdot 6H_2O$ (8.11 g, 0.03 mol) and $CH_3COONa3H_2O$ (8.16 g, 0.06 mol) in 10 mL of hot water[18], respectively. Mix the prepared solutions and heat to 50°, maintaining the temperature for 30 minutes. Allow the mixture to crystallize naturally in air for 72 hours, resulting in deep red prismatic crystals, which are basic iron acetate. A photograph of the basic iron acetate is shown in Fig. 2.

Fig. 2 Photograph of basic iron acetate

Synthesis of PW9 O34

Weigh 9.7027 grams[19] of sodium tungstate dihydrate and 0.8186 grams of disodium hydrogen phosphate, and dissolve these two compounds in 100 mL of distilled water. Then, adjust the pH of the solution to 9 using 37% hydrochloric acid. Next, use a centrifuge to remove impurities. Allow the required salt to crystallize at 5° for 3 days. Collect the white crystals, wash them with cold water, and dry them under vacuum to obtain a white solid PW_9O_{34}.

Synthesis of $Fe_3PW_9O_{34}$

Prepare 1.23 mmol of $Fe_3PW_9O_{34}$ solution and 4.11 mmol of ferric acetate solution, then mix them. Use a rotary evaporator to dry, obtaining a white solid, which is the $Fe_3PW_9O_{34}$ formed after coordination[20].

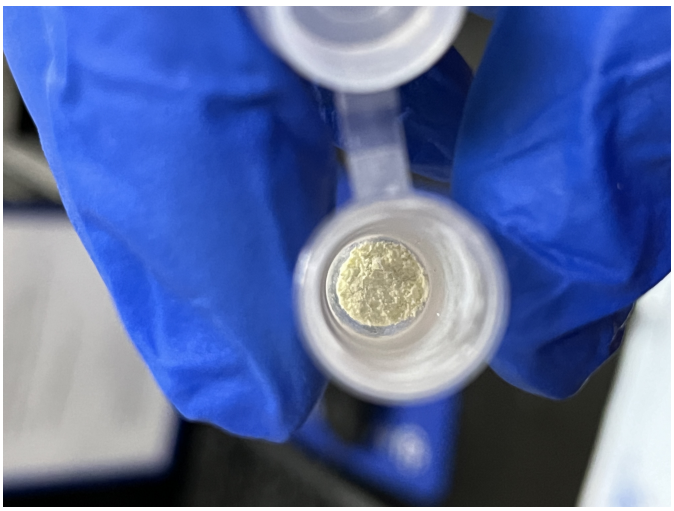

Fig. 3 Image of $Fe_3PW_9O_{34}$

Structural Characterization and Catalytic Reaction Monitoring

System overview

This section will introduce how various characterization techniques were applied to determine the identity and structure of the synthesized substances, validate the feasibility of the synthetic route presented in this study, and explore the potential applications and related information of the synthesized materials.

Mass Spectrometry Testing

In this study, mass spectrometry analysis of the catalysts before and after coordination was performed using Electrospray Ionization (ESI)[21]. First, $Fe_3PW_9O_{34}$ and PW_9O_{34} were dissolved in appropriate solvents, with the solution concentration controlled at approximately 1 mg/mL to ensure good signal intensity and ionization efficiency. The prepared solution was then introduced into the mass spectrometer, where ionization occurred under vacuum conditions. The ionized sample molecules were separated in the mass analyzer based on their mass-to-charge ratio (m/z), and the detector recorded and generated the corresponding mass spectrum. By analyzing the mass spectrum, the molecular weight and structural information were determined based on the m/z and isotope distribution pattern. Additionally, the characteristic peaks in the mass spectrum were used to further confirm the structural composition of the sample.

0.0.1 Fourier Transform Infrared Spectroscopy (FTIR) Testing

The catalysts before and after coordination were analyzed using a Fourier Transform Infrared Spectrometer (FTIR) for infrared spectrum scanning. First, the catalyst PW_9O_{34} before coordination was ground with KBr to form a transparent thin film, ensuring good light path transparency. The wavenumber range was set from 4000 to 400 cm^{-1}, with 32 scans and a resolution of 4 cm^{-1} to ensure the accuracy and reproducibility of the spectrum. During measurement, care was taken to avoid exposing the sample to moisture and air, preventing interference from hygroscopic substances. After data collection, the peaks were calibrated using spectral analysis software, and key absorption peaks were assigned to determine the molecular structural characteristics of the sample. The distribution and intensity of the infrared characteristic peaks were further used to confirm the functional groups and structural composition within the molecule.

Crystal 3D Structure Based on Single-Crystal X-Ray Diffraction

Single crystals of ferric acetate with appropriate size were selected, typically ranging from 0.1 to 0.3 mm to ensure good diffraction performance. The single crystal was fixed on the sample stage of the X-ray diffractometer, with low-temperature conditions (e.g., 100 K) applied to maintain crystal stability and prevent radiation damage and thermal motion effects. X-rays generated from the X-ray source were diffracted by the single crystal sample, and specific diffraction peaks were generated for each crystal face based on Bragg's Law ($n\lambda = 2dsin\theta$). The detector received and recorded the intensity and position of each diffraction peak, forming a complete diffraction dataset. Through Fourier transformation and structural refinement of the data, the electron density distribution of the sample was obtained, enabling the determination of atomic positions and their relative relationships. Finally, using the professional software Olex2, the model was optimized, completing the structure analysis and generating a 3D molecular or crystal structure diagram[22].

Comparing the Optimistic Catalytic Condition of the 2,4-Dihydroxybenzaldehyde and Diisopropyl Azodicarboxylate Addition Reaction Using Ambient Mass Spectrometry

Accurately weigh 13.8 mg of solid 2,4-dihydroxybenzaldehyde and dissolve it in 5 mL methanol to prepare a 20 mM solution (Solution 1) with continuous stirring. Take 939 μL of diisopropyl azodicarboxylate and dissolve it in 5 mL methanol to prepare a 1 mM solution (Solution 2). Accurately weigh 0.5 mg of $Fe_3PW_9O_{34}$ and dissolve it in 5 mL methanol to prepare a 0.1 mg/mL solution (Solution 3), storing it in the dark. Accurately weigh 0.5 mg of basic iron acetate and dissolve it in 5 mL methanol to prepare a 0.1 mg/mL solution (Solution 4), storing it in the dark.

Mix 500 μL of Solution 1 and 100 μL of Solution 2 in a reaction vial, then add methanol to make the total volume 10 mL. A homemade electrospray ionization (ESI) microdroplet reaction system was used to facilitate the reaction of the reactants in the microdroplets, and the contents were monitored after 5 minutes by mass spectrometry.

Mix 500 μL of Solution 1, 100 μL of Solution 2, and 500 μL of Solution 3 in a reaction vial, then add methanol to make the total volume 10 mL. A homemade electrospray ionization (ESI) microdroplet reaction system was used to facilitate the reaction of the reactants in the microdroplets, and the contents were monitored after 5 minutes by mass spectrometry.

Mix 500 μL of Solution 1, 100 μL of Solution 2, and 500 μL of Solution 4 in a reaction vial, then add methanol to make the total volume 10 mL. A homemade electrospray ionization (ESI) microdroplet reaction system was used to facilitate the reaction of the reactants in the microdroplets, and the contents were monitored after 5 minutes by mass spectrometry.

Monitoring of the 2,4-Dihydroxybenzaldehyde and Diisopropyl Azodicarboxylate Addition Reaction Catalyzed by $Fe_3PW_9O_{34}$ Using Ambient Mass Spectrometry

Accurately weigh 13.8 mg of solid 2,4-dihydroxybenzaldehyde and dissolve it in 5 mL methanol to prepare a 20 mM solution (Solution 1) with continuous stirring. Take 939 μL of diisopropyl azodicarboxylate and dissolve it in 5 mL methanol to prepare a 1 mM solution (Solution 2).

Accurately weigh 0.5 mg of $Fe_3PW_9O_{34}$ and dissolve it in 5 mL methanol to prepare a 0.1 mg/mL solution (Solution 3), storing it in the dark. Mix 500 μL of Solution 1, 100 μL of Solution 2, and 500 μL of Solution 3 in a reaction vial, then add methanol to make the total volume 10 mL. The concentrations in the reaction system are as follows: 2,4-dihydroxybenzaldehyde at 1 mM, diisopropyl azodicarboxylate at 0.1 mM, and the catalyst $Fe_3PW_9O_{34}$ at 0.1 mg/mL.

A homemade electrospray ionization (ESI) microdroplet reaction system was used to facilitate the reaction of the reactants in the microdroplets, and the intermediates and reaction progress were monitored in real-time by mass spectrometry. Collision-induced dissociation (CID) was used to analyze and identify the intermediate and the product. The operational parameters were as follows: Full-scan ion spectra from m/z 50 to 1000 in negative ion mode. The maximum ion injection time was 1000 ms. All mass spectrometry data were acquired and processed using Xcalibur software. During the reaction, care was taken to avoid decomposition of diisopropyl azodicarboxylate upon heating, and cooling water was passed through to maintain a low reaction temperature.

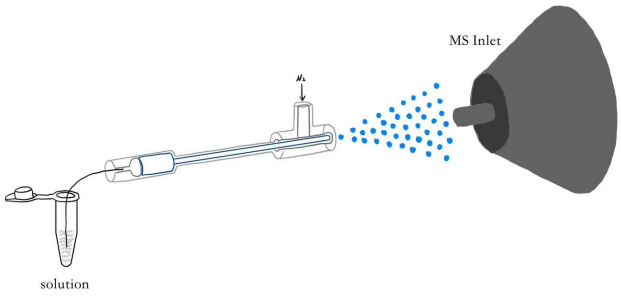

Fig. 4 Schematic Diagram of the Homemade Ion Source Device

Results and Discussion

Analysis of the Fourier Transform Infrared Spectroscopy (FTIR) Results of PW_9O_{34}

Based on the analysis of the Fourier Transform Infrared Spectroscopy (FTIR) spectrum (Figure 5), the characteristic features of the sample with the chemical formula PW_9O_{34} can be confirmed. The absorption peak at 1400 cm^{-1} corresponds to the asymmetric stretching vibration of the PO bond in the PO unit of the anion. The peak at 1160 cm^{-1} is attributed to the asymmetric stretching vibration of the WOW bridging oxygen. The 1060 cm^{-1} peak represents the symmetric stretching vibration of the PO bond. The strong peak at 1015 cm^{-1} corresponds to the stretching vibration of the terminal W=O bond and is a characteristic peak of the Keggin structural unit. The shoulder peak at 995 cm^{-1} also corresponds to the W=O terminal oxygen stretching vibration. The 940 cm^{-1} peak is due to the symmetric stretching vibration of the WOW bridging oxygen. In the region of 890600 cm^{-1}, the absorption bands are attributed to the bending vibrations of the WOW bridging oxygen. Finally, the peaks at 510 and 460 cm^{-1} correspond to the bending vibrations of the WO bonds. In summary, the infrared characteristic peak positions and intensities of the measured sample align with those of PW_9O_{34}, confirming the molecular structure of the sample.

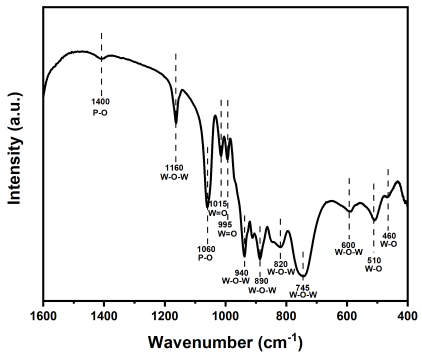

Fig. 5 Fourier Transform Infrared Spectroscopy (FTIR) Spectrum of PW_9O_{34}

Analysis of the ESI Mass Spectrometry Test Results of $Fe_3PW_9O_{34}$ and PW_9O_{34}

Mass spectrometry analysis confirmed the composition and structure of the synthesized compounds. The Electrospray Ionization Mass Spectrometry (ESI-MS) results revealed several major ion peaks for $Fe_3PW_9O_{34}$ and PW_9O_{34}. During the test, the substances randomly interacted with Na^+, K^+, and H^+ ions to form negative ions. High-resolution scans of several prominent peaks were performed, and the spectra were analyzed, revealing several abundant negative ions. After comparison, the composition and structure of the synthesized $Fe_3PW_9O_{34}$ and PW_9O_{34} were confirmed.

Figure 6 shows a high peak at m/z around 1175. Analysis of this peak revealed negative ions including $H_{11}KNaO_{37}PW_9^{2-}$ (m/z = 1174.69/1176.70), which were generated by the random combination of PW_9O_{34} with Na^+, K^+, and H^+ ions.

Figure 7 shows two high peaks at mass-to-charge ratios (m/z) around 1395 and 1385. Analysis of the peak at m/z 1395 revealed negative ions including $Fe_3H_{10}K_6NaO_{42}PW_9^{2-}$ (m/z = 1395.49/1394.99/1395.99), which were formed by the random combination of $Fe_3PW_9O_{34}$ with Na^+, K^+, and H^+ ions. The peak around m/z 1485 revealed negative ions including FeHKOPW (m/z = 1387.47/1384.96/1385.41), formed in a similar manner.

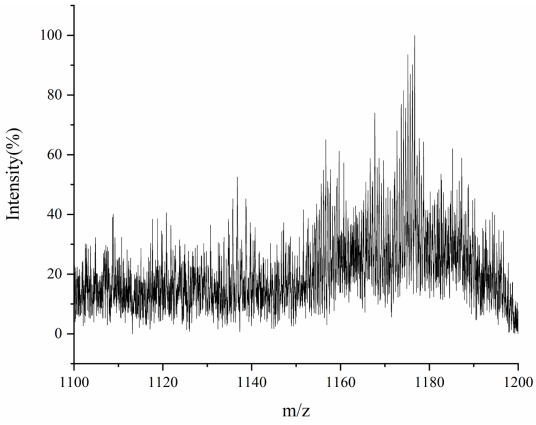

Fig. 6 Mass Spectrum of $Fe_3PW_9O_{34}$

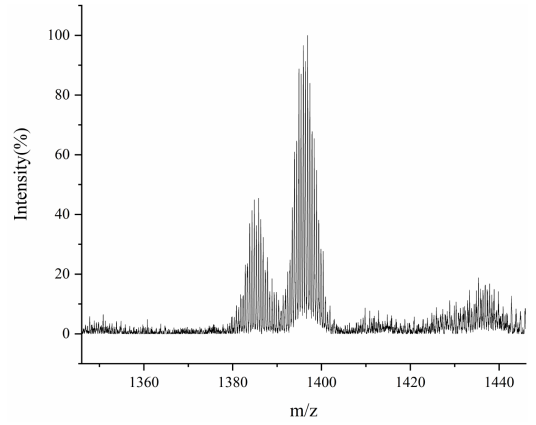

Fig. 7 Mass Spectrum of PW_9O_{34}

Crystal 3D Structure Diagram Based on Single-Crystal X-Ray Diffraction

Based on the analysis of the single-crystal X-ray diffraction data of the ferric acetate crystal, the molecule exhibits a typical octahedral coordination structure, where iron (Fe) atoms form coordination bonds with acetate (CH_3COO^-) ligands through oxygen (O) atoms. The Fe-O bond lengths in the molecule are evenly distributed, indicating a high degree of symmetry and structural stability. The acetate ligands are linked in a bridging manner, connecting multiple iron atoms and forming a stable cyclic structure. This bridging mode is common in basic acetate metal compounds and imparts certain polymeric characteristics to the molecule. Additionally, hydrogen bonds are present in the molecular structure, which further enhance the intermolecular interactions, thereby stabilizing the crystal structure. Chlorine (Cl) ions are also observed on the molecular periphery, where they interact electrostatically with the coordination center, helping maintain the integrity of the crystal.

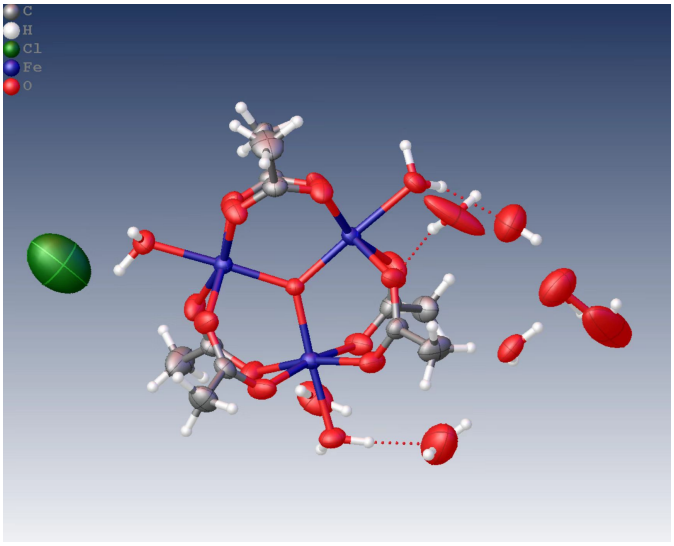

Fig. 8 Single-Crystal 3D Structure Diagram of Ferric Acetate

The Optimistic Catalytic Condition of the 2,4-Dihydroxybenzaldehyde and Diisopropyl Azodicarboxylate Addition Reaction Using Ambient Mass Spectrometry

The product will not produced if microdroplets is not used no matter the presence or the absence of catalyst if no other catalytic factors are invited[23]. Based on the results of mass spectrometry, given that microdroplets are facilitating the reaction, the product with 339 m/z is not detected in the absence of catalyst. Based on the results of mass spectrometry, given that microdroplets are facilitating the reaction, the product with 339 m/z is detected with a relative abundance 30% relative to the abundance of 2,4-Dihydroxybenzaldehyde in the presence of $Fe_3PW_9O_{34}$ as a catalyst. Based on the results of mass spectrometry, given that microdroplets are facilitating the reaction, the product with 339 m/z is detected with a relative abundance 15% relative to the abundance of 2,4-Dihydroxybenzaldehyde in the presence of basic iron acetate as a catalyst.

The difference in abundance of the product between the reac-

tion catalyzed by $Fe_3PW_9O_{34}$ and basic iron acetate may due to $Fe_3PW_9O_{34}$'s distinct structure. In addition to iron as the active center, it also contains a polyoxometalate skeleton with electronic regulation and acidic functions. This skeleton not only stabilizes iron atoms, preventing their aggregation or loss, but also enhances the activity and selectivity of catalytic reactions through synergistic effects.

Reaction Mechanism of $Fe_3PW_9O_{34}$ Catalyzed Addition Reaction of 2,4-Dihydroxybenzaldehyde and Diisopropyl Azodicarboxylate

Based on the results of ambient mass spectrometry monitoring the catalytic reaction process, the mechanism of C-H bond activation and C-N coupling was determined. Before the reaction system liquid was introduced, the ion peak at m/z = 339 was absent. However, after introducing the reaction system liquid, this peak gradually increased, suggesting that the substance was probably the expected product. During product monitoring, aside from peaks corresponding to the reactants, products, and catalyst, several other ion peaks were observed in the mass spectrum. Based on organic chemistry theory, these substances are likely intermediates in the reaction. A detailed analysis of the mass spectrometric signals, along with organic chemistry knowledge, allowed for the structural prediction of the intermediates. Based on these predicted structures, the reaction mechanism of $Fe_3PW_9O_{34}$ catalyzed addition of 2,4-dihydroxybenzaldehyde and diisopropyl azodicarboxylate was proposed, as shown in Figure 9. First, under the catalysis of $Fe_3PW_9O_{34}$, 2,4-dihydroxybenzaldehyde loses a hydrogen atom from the aldehyde group, forming an R radical. Then, this radical undergoes an addition reaction with the electrophilic diisopropyl azodicarboxylate, where the N=N bond in the azodicarboxylate breaks. One nitrogen atom forms a bond with the R radical, while the other nitrogen atom becomes a free radical with an unpaired electron. This nitrogen radical further abstracts an H atom, ultimately yielding the product. The product's Collision-induced dissociation (CID) pattern is shown in Figure 10, and its lysis pathway analysis is presented in Figure 11. The pattern shows that the product is exactly what the researcher expect. The researcher also tried to use MS^2 to identify and confirm that production of the intermediate. However, the intermediate this paper proposed is 2,4-dihydroxybenzaldehyde that lost a hydrogen. As such, the MS^2 pattern cannot confirm whether the intermediate is produced since it's MS^2 pattern is very similar to that of 2,4-dihydroxybenzaldehyde. Nevertheless, it is very likely that it's structure is what the paper proposed because the pattern shows proper cleavage fragments of both 2,4-dihydroxybenzaldehyde and the intermediate, and the peak m/z=136 is present.

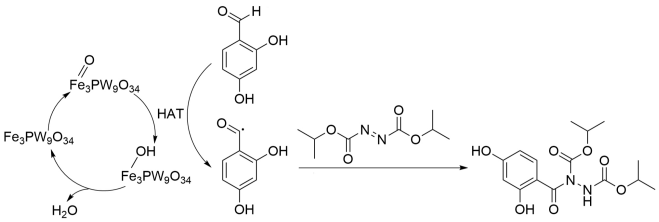

Fig. 9 Reaction Mechanism Diagram of $Fe_3PW_9O_{34}$ Catalyzed Addition Reaction of 2,4-Dihydroxybenzaldehyde and Diisopropyl Azodicarboxylate

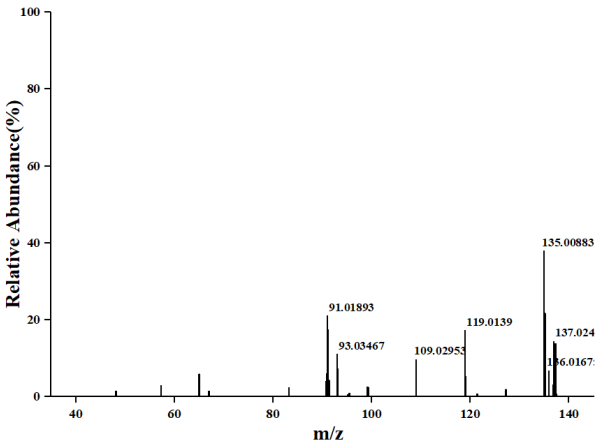

Fig. 10 MS^2 Pattern of the Product

Future Works

Although this study has offered a novel catalyst choice, proposed a likely mechanism of a certain kind of reaction, and explored a creative and cutting-edge method that monitors reactions, it has some limitations that could be addressed in future work.

From the outset, the synthesis route of the catalyst described in this study has not yet been confirmed the purity due to insufficient experimental equipment, which suggests that future

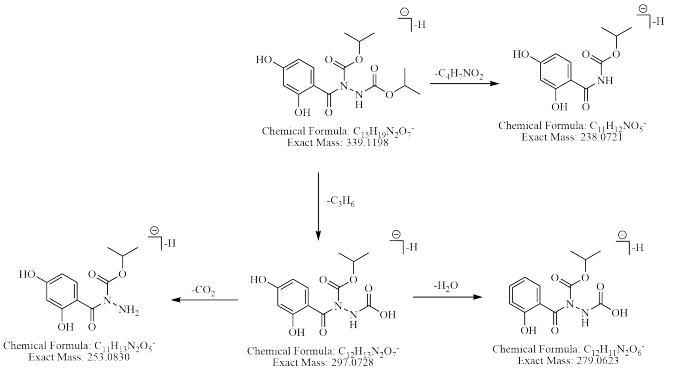

Fig. 11 The Product's Cleavage Pathway Analysis based on MS^2

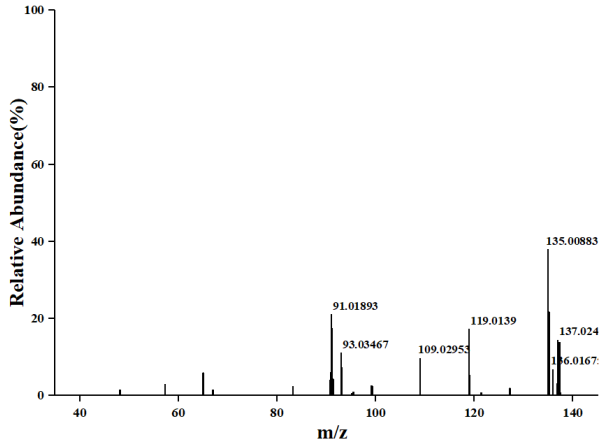

Fig. 12 MS^2 Pattern of the Intermediate

research should introduce equipment that can determine the product's purity like High-Performance Liquid Chromatography to yield the synthesis route's productivity.

Furthermore, this work is limited by the number of reactions studied, thus further studies should use the method this research proposed to study more reactions to not only confirm the method's usefulness but also expand human knowledge on mechanisms.

Finally, future research could focus on controlling microdroplets' properties, which would benefit the scientific exploration of the secret of the impressive catalytic effect of microdroplets, as well as further broaden people's understanding of the reaction monitoring method proposed in this study.

Conclusion

In this study, we successfully synthesized $FE_3PW_9O_{34}$ and validated the feasibility of the synthesis route using various characterization methods. The characterization results in this paper

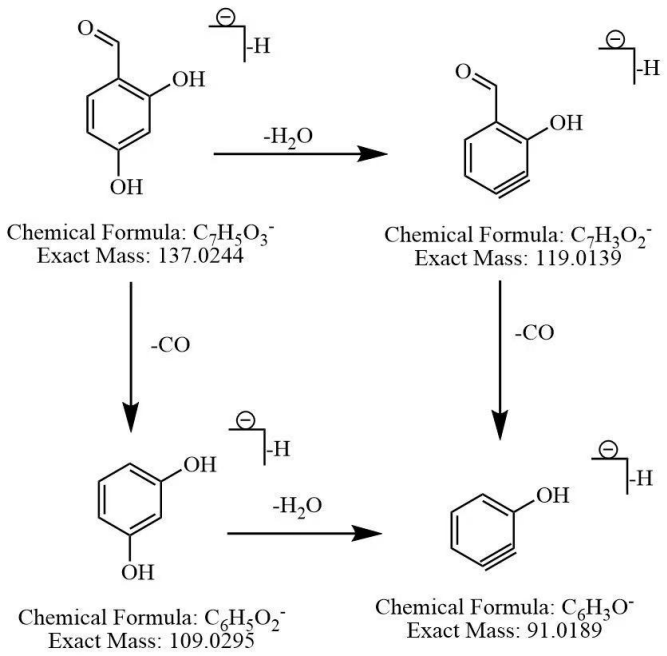

Fig. 13 The Intermediate's Cleavage Pathway Analysis based MS^2 Pattern

demonstrate that, based on the original tungsten-phosphorus heteropolyacid, $FE_3PW_9O_{34}$ successfully extends its redox-active sites by introducing FE^{3+}. Additionally, a reaction pathway was developed based on water microdroplets and the $FE_3PW_9O_{34}$ catalyst, which allows the addition reaction of 2,4-dihydroxybenzaldehyde and diisopropyl azodicarboxylate to occur spontaneously in ambient conditions without the need for external factors like photoelectric catalysts. Furthermore, the intermediate of this reaction was studied via Ambient mass spectrometry, and a possible reaction mechanism was proposed. Moreover, $FE_3PW_9O_{34}$ exhibited excellent stability and functionality, suggesting its broad application potential not only for the catalytic addition reaction of 2,4-dihydroxybenzaldehyde and diisopropyl azodicarboxylate discussed in this study but also in other oxidation reactions and heterogeneous catalysis, such as pollutant degradation.

This study provides a new approach for the design of functionalized heteropoly acids, laying the foundation for exploring their applications in green chemistry and energy fields. Future research can further adjust the metal coordination environment to optimize catalytic performance, thereby achieving more efficient catalytic cycles, or focus on the material's application potential outside the catalytic field. Furthermore, the proposed hypothetical reaction mechanism in this study not only offers inspiration and guidance for subsequent research on the addition reaction of 2,4-dihydroxybenzaldehyde and diisopropyl azodicarboxylate or related reactions, but also provides an efficient and low-energy approach for studying such organic reactions,

laying the groundwork for future research to be conducted in a greener and simpler manner.

Acknowledgement

The author thanks Beijing Normal University for providing him labs and apparatus, and PhD student Xiyang Ge's assist on safe usage of mass spectrometry. The Author thanks Professor Nana for guidance on the analytic chemistry knowledge.

References

1 X. Song, Y. Meng and R. N. Zare, *Journal of the American Chemical Society*, 2022, **144**, 16744–16748.

2 C. Gong, D. Li, X. Li, D. Zhang, D. Xing, L. Zhao, X. Yuan and X. Zhang, *Journal of the American Chemical Society*, 2022, **144**, 3510–3516.

3 X. Ge, Y. Yin, J. Ouyang and N. Na, *Acta Mass Spectrometrica*, 2024, **1**, 31–43.

4 Y. Meng, E. Gnanamani and R. N. Zare, *Journal of the American Chemical Society*, 2023, **145**, 7724–7728.

5 Y. Zhu, S. Guo, N. Zhuang, Q. Ping, J. Zhang, Z. An, H. Song, X. Shu, W. Xi, L. Zheng, R. Zhang and J. He, *ACS Catalysis*, 2023, **14**, 56–66.

6 Y. Meng, E. Gnanamani and R. N. Zare, *Journal of the American Chemical Society*, 2022, **145**, 32–36.

7 Y. Zhao, F. Wu, Y. Miao, C. Zhou, N. Xu, R. Shi, L. Wu, J. Tang and T. Zhang, *Angewandte Chemie International Edition*, 2021, **60**, 21728–21731.

8 S. Esposti, D. Dondi, M. Fagnoni and A. Albini, *ChemInform*, 2007, **38**, year.

9 L. Liu, R. Huang, Z. Zhang, X. Wei, Y. Bai and Y. Zhu, *Acta Moleculorum Science*, 2006, **6**, 361–366.

10 J.-C. Raabe, T. Esser, F. Jameel, M. Stein, J. Albert and M. J. Poller, *Inorganic Chemistry Frontiers*, 2023, **10**, 4854–4868.

11 D. Azaiza-Dabbah, C. Vogt, F. Wang, A. Masip-Snchez, C. de Graaf, J. M. Poblet, E. Haviv and R. Neumann, *Angewandte Chemie International Edition*, 2021, **61**, year.

12 R. I. Demian, N. E. Manicke, A. L. Rusine and R. G. Cooks, *Rapid Communications in Mass Spectrometry*, 2008, **22**, year.

13 J. Qin, J. Ouyang and N. Na, *Acta Mass Spectrometrica*, 2023, **2**, 158–169.

14 S. D. Brown, T. A. Betley and J. C. Peters, *Journal of the American Chemical Society*, 2002, **125**, 322–323.

15 C. Li, N. Mizuno, K. Yamaguchi and K. Suzuki, *Journal of the American Chemical Society*, 2019, **141**, 7687–7692.

16 Q. Zhang, J. Cheng, Y. Zhao and Y. Zhang, *Fine Chemicals*, 2023, 1–13.

17 I. B. Perry, T. F. Brewer, D. W. C. MacMillan *et al.*, *Nature*, 2018, **560**, 70.

18 P. Li, *MSc thesis*, Yantai University, 2023.

19 C. Wang, *MSc thesis*, Taiyuan University of Technology, 2023.

20 Y. Song, L. Li, P. Wang, X. Wu and C. Ma, *Journal of Atomic and Molecular Physics*, 2024, **4**, 173–178.

21 D. Dondi, M. Fagnoni, A. Molinari, A. Maldotti and A. Albini, *Chemistry (Weinheim an der Bergstrasse, Germany)*, 2004, **10**, year.

22 Z. Long, J. Li, Z. Tang, J. Sun, Y. Gao and N. Na, *Chemical Education (Chinese and English)*, 2022, **16**, 86–91.

23 K. Zhao, *MSc thesis*, Zhongyuan University of Technology, 2024.